Buoyant formation number of a starting buoyant jet

Ruo-Qian Wang,[1] Adrian Wing-Keung Law,[2] E. Eric Adams,[3] and Oliver B. Fringer[4]
[1]*Singapore-MIT Alliance for Research and Technology, Singapore 117543, Singapore*
[2]*School of Civil and Environmental Engineering, Nanyang Technological University, Singapore 639798, Singapore*
[3]*Department of Civil and Environmental Engineering, Massachusetts Institute of Technology, Massachusetts 02139, USA*
[4]*Environmental Fluid Mechanics Laboratory, Stanford University, California 94305-4020, USA*

(Received 19 May 2009; accepted 27 October 2009; published online 29 December 2009)

Understanding the influence of buoyancy on the formation number is important for analyzing the development of a starting buoyant jet and the interactions between its vortex ring and trailing stem. Numerical simulations with a large-eddy simulation model are performed to reproduce the starting buoyant jet in conditions ranging from pure jet to lazy plume. From the results, an improved method to determine the formation number is proposed based on the occurrence of a step jump in the vortex ring circulation. A comparison of the numerical results with the experimental data for a starting pure jet is first performed. The widely accepted formation number ($\approx$4.0) is obtained, which implies that the method is satisfactory. The effect of buoyancy on the formation number is then investigated for two turbulent discharge conditions of Re=2000 and 2500 and with a wide range of buoyancy flux. Best-fit results are obtained that correlate the formation number with the Richardson number. Finally, a slug model that incorporates buoyancy is developed to allow prediction of the "buoyant formation number" for the starting buoyant jet using a limiting value of 0.33 for the dimensionless energy, which is the same value for a pure jet. © *2009 American Institute of Physics*.
[doi:10.1063/1.3275849]

I. INTRODUCTION

Starting buoyant intrusions are common in natural and engineered systems and span multiple time and length scales. Examples include volcanic eruptions, piston engine fuel injection, delivery of scent to a theater through an air canon,[1] and microscale heat exchange in microelectromechanical systems. The significance of such intrusions has drawn numerous studies in the past to understand and quantify their behavior (see Ref. 2).

A significant aspect of the starting buoyant intrusion is the relationship between the starting head vortex and the trailing stem formation. The behavior of the starting head vortex closely resembles a discrete vortex ring, which has been extensively studied (a good recent summary can be found in Ref. 3). Yet the phenomenon cannot be examined solely by the starting vortex as the trailing stem can continue to feed mass, circulation, and energy to the vortex. A well known illustrative example is provided by Gharib *et al.*,[2] who performed an experimental study on the vortex ring generated by a piston/cylinder arrangement. They showed that two distinct states exist depending on the "formation time," t_f, which is defined as the ratio of the stroke distance over the nozzle diameter, L/D. Note that t_f is referred to as a nondimensional time because it is the ratio of the release time, L/U_0, where U_0 is the release velocity, divided by the time, D/U_0, required for the released fluid to travel a distance D. With a short formation time of 2, an isolated vortex ring was formed without the development of a trailing stem (i.e., the intrusion was totally absorbed in the starting vortex), whereas with a longer formation time of 14.5, the trailing stem was observed following the front vortex ring. The critical value of the formation time was called the "formation number," above which a trailing stem is present. They found that the formation number is approximately equal to 4.0 and is relatively invariant through various nozzle conditions and velocity histories. The formation number was proposed as the criterion for the "pinch-off" occurrence (i.e., detachment of the starting head vortex from trailing stem). This is because the starting vortex could not absorb the additional intrusion from the piston if the formation time was higher than the formation number and would physically separate from the trailing stem. In other words, when the formation number is reached, the vortex ring has reached the upper limit of circulation by the driving mechanism.[2]

The existence of the formation number has also been confirmed by numerical simulations. Rosenfeld *et al.*[4] simulated the formation of nonbuoyant vortex rings by symmetrical laminar flow configurations and observed the different flow structures below and above the formation number. They reported that the formation number was strongly affected by the initial velocity profile but less by the velocity history, while Zhao *et al.*[5] clearly illustrated the circulation absorption process between the vortex ring and the trailing stem. Mohseni *et al.*[6] extended the simulation to include a variety of nonconservative body forces and concluded that a varying nozzle diameter can delay the pinch-off. Their work stimulated an interest to further examine nozzles with changing diameters, such as those studied by Dabiri and Gharib[7] and Allen and Naitoh.[8]

Taking advantage of the observations and understandings from these numerical and experimental studies, quantitative models were developed to describe the initial starting behavior. They include Mohseni and Gharib,[9] Linden and

 © 2009 American Institute of Physics

Downloaded 23 Feb 2010 to 171.67.216.23. Redistribution subject to AIP license or copyright; see http://pof.aip.org/pof/copyright.jsp

Turner,[10] Mohseni,[11] Kaplanski and Rudi,[12] and Shusser *et al.*[13] Gharib *et al.*[2] defined a dimensionless energy $E_{nd}=E/\sqrt{\rho I\Gamma}=\sqrt{\pi/2}(D/L)$, where E, Γ, and I are the kinetic energy, circulation, and impulse of the starting jet (detailed further in Sec. IV C). They calculated a limiting value of E_{nd}, or E_{lim}, to be 0.33 (referred to as α in their paper), below which pinch-off would occur. Since $E_{nd}=0.33$ corresponds to $L/D=3.8$, pinch-off would thus occur for L/D greater than about 4. Analytically, they demonstrated that E_{lim} represents a level beyond which the piston cannot deliver more energy, circulation, and impulse to the starting vortex steadily according to the Kelvin-Benjamin variational principle.[14] Mohseni and Gharib[9] formulated a model to describe the phenomenon of the formation number based on the Norbury's family of vortices and the slug model, which was extended to various piston velocity programs by Shusser *et al.*[13] Similarly, Linden and Turner[10] matched the properties of the injected plug of fluid and the Norbury's family of vortices to show that E_{lim} reflects the constraint due to the volume limitation of the vortex ring core. Kaplanski and Rudi[12] refined the model of Linden and Turner[11] by incorporating the viscosity.

Most studies on the starting phenomenon so far have focused on nonbuoyant intrusions with the piston-cylindrical configuration. The equivalent situation of a starting buoyant jet with a strong buoyancy component (in cases such as the eruption of a volcano and open-water disposal of a sediment mass whereby the buoyancy effect is prevalent due to the large density difference between the intrusion and ambient fluid) has not been well investigated. For the asymptotic case of a thermal (lazy plume without initial momentum), Pottebaum and Gharib[15] confirmed the existence of the maximum circulation by performing experiments with plumes generated by a heat disk; and Shusser and Gharib[16] suggested based on an analytical model that the equivalent formation number would be $\tau=4.73$, where τ is the duration of the release divided by the characteristic time $T_0=\sqrt{D/2g'}$ required for an effective gravitational force of g' to accelerate the mass a distance equal to the cylinder diameter D.

Neither the starting pure jet models (e.g., Mohseni and Gharib[9]) nor the starting thermal models (e.g., Shusser and Gharib[16]) are able to fully address the dynamics of a starting buoyant jet with a combination of initial momentum and buoyancy fluxes. As far as the formation number is concerned, it is not clear *a priori* whether the initial buoyancy would delay or speed up the pinch-off process after the turbulent intrusion occurs. In addition, at present the formats of the formation time and formation number are distinctly different between the existing pure jets and thermal models. A suitable analytical model that can bridge the two asymptotic cases and cover the buoyant jet situation would be highly desirable. It is noted that such unified analyses have been conducted for steady state buoyant jets (e.g., Wang and Law[17]), but a similar investigation for starting buoyant jets has not been reported in literature as far as the authors are aware.

In this study, a series of numerical experiments is performed using the large-eddy simulation (LES) approach to examine the formation dynamics of a starting buoyant jet. In the following, the numerical approach and the flow configuration are first introduced in Sec. II. In Sec. III, the numerical model is verified with the asymptotic case of a starting pure jet, for which the experimental data regarding the formation process have been reported previously in literature. Subsequently, extensive simulations are performed covering a broad range between the pure jet and the lazy plume in Sec. IV, and a slug model is developed to include the buoyancy effect on the formation number. Finally, the conclusions from the current study are listed in Sec. V.

II. NUMERICAL MODEL

A. Governing equations

The governing equations of the grid-filtered continuity, Navier–Stokes, and temperature transport equations with the Boussinesq approximation can be expressed as follows:[18]

$$\frac{\partial \bar{u}_i}{\partial x_i}=0, \tag{1}$$

$$\frac{\partial \bar{u}_i}{\partial t}+\frac{\partial \bar{F}_{ij}}{\partial x_j}=\bar{S}_i, \tag{2}$$

$$\frac{\partial \bar{\phi}}{\partial t}+\frac{\partial \bar{R}_j}{\partial x_j}=0, \tag{3}$$

where

$$\bar{F}_{ij}=\bar{u}_i\bar{u}_j+\bar{p}\,\delta_{ij}-\nu\frac{\partial \bar{u}_i}{\partial x_j}+\tau_{ij}, \tag{4}$$

$$\bar{S}_1=-g\beta(\bar{\phi}-\phi_0)\delta_{i3}+f(-\bar{u}_2\delta_{i1}+\bar{u}_1\delta_{i2}), \tag{5}$$

$$\bar{R}_j=\bar{u}_j\bar{\phi}-\kappa\frac{\partial \bar{\phi}}{\partial x_j}+\chi_j. \tag{6}$$

In the above equations, the overbar variables represent the grid-filtered quantities. t is time, u_i $(i=1,2,3)$ are the Cartesian velocity components in the direction of x, y, and z. Other quantities are defined as follows: p is the pressure, g is the gravity, ϕ is the temperature, ϕ_0 is the background temperature, $\beta=(1/\phi_0)(\partial\rho/\partial\phi)$ is the coefficient of thermal expansion, ν is the kinematic viscosity, and κ is the thermal diffusivity. Note that all the equations are subjected to the Einstein rule of summation.

The subgrid terms τ_{ij} and χ_j are specified as

$$\tau_{ij}=\overline{u_iu_j}-\bar{u}_i\bar{u}_j, \tag{7}$$

$$\chi_j=\overline{u_j\phi}-\bar{u}_j\bar{\phi}. \tag{8}$$

These two terms can be modeled by the dynamic mixed subgrid-scale model, the details of which can be found in Refs. 19 and 20.

The governing equations are discretized by a finite volume formulation on a single nonstaggered grid.[19] Various discretization schemes are applied: (1) a semi-implicit scheme with Crank–Nicholson method on the diagonal viscous and diffusive terms, and Adams–Bashforth method on

Downloaded 23 Feb 2010 to 171.67.216.23. Redistribution subject to AIP license or copyright; see http://pof.aip.org/pof/copyright.jsp

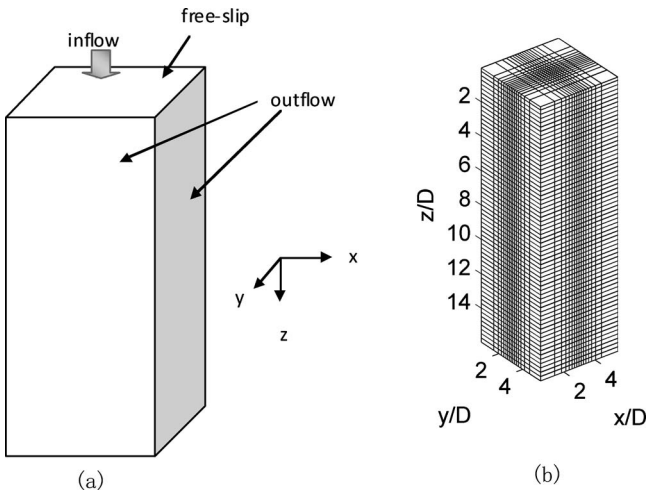

FIG. 1. The computational domain.

the other terms in time; (2) accurate upwind-difference schemes on the convective terms; and (3) second-order central difference on all the other spatial differential terms. The convective terms of the momentum equations [Eq. (2)] are discretized using the QUICK scheme to minimize the expense of computation, whereas the convective terms of the scalar transport equation [Eq. (3)] are discretized using the SHARP scheme to avoid spurious oscillation.[19,21]

The numerical model has been verified by a series of comparisons with standard experiments, e.g., Cui and Street,[22] and implemented in recent studies.[23–26] The parallel code used in the present study was developed by Cui and Street.[22]

B. Flow configuration

The computational domain is three dimensional with a square horizontal cross section that extends $0.3\times0.3\times0.8$ m^3 in the Cartesian coordinates x, y, and z respectively [Fig. 1(a)]. The starting buoyant jet is issued downward from the top boundary with a uniform velocity U_0 into a homogeneous and stationary ambient fluid through a circular nozzle with a diameter of $D=5$ cm. Thus, the computation domain is equivalent to a size of $6D\times6D\times16D$, which has been verified to be sufficient for the investigation of the near-field formation process.[25] The buoyant jet is heavier than the ambient and with a relative density difference of $\Delta\rho_0/\rho_0$ (thus the buoyant action is in the same direction as the plume injection). The governing equations are discretized into a stretched mesh, which has denser grids at the center axis through the nozzle [as shown in Fig. 1(b)].

Before the simulation begins, the fluid in the computational domain is stagnant with a uniform density ρ_0. The boundary conditions are depicted in Fig. 1(a). The top boundary is a free-slip surface permitting no vertical through flow, while the other boundaries are "no-gradient" outflow boundaries following the recommendation of Yuan.[26] A constant volume flux, determined from the prescribed inflow velocity U_0, is then imposed at the inlet at $t=0$ to initiate the simulation.

To facilitate the analysis, some characteristic parameters are defined following Fischer *et al.*,[27]

$$Q_0=\frac{1}{4}\pi D^2U_0,\quad M_0=\frac{1}{4}\pi D^2U_0^2,$$

$$B_0=\frac{1}{4}\pi g\frac{\Delta\rho_0}{\rho_0}D^2U_0,\quad l_M=\frac{M_0^{3/4}}{B_0^{1/2}},\quad l_Q=\frac{Q_0}{M_0^{1/2}},$$

$$R_0=\frac{l_Q}{l_M}=\frac{Q_0B_0^{1/2}}{M_0^{5/4}}=\left(\frac{\pi}{4}\right)^{1/4}\left(\frac{g'D}{U_0^2}\right)^{1/2}=\left(\frac{\pi}{4}\right)^{1/4}\frac{1}{F_d},\tag{9}$$

$$\mathrm{Re}=\frac{U_0D}{\nu},$$

where Q_0, M_0, and B_0 are initial volume flux, momentum flux, and kinematic buoyancy flux, respectively, g' is reduced gravity $(g\Delta\rho_0/\rho_0)$, $\Delta\rho_0/\rho_0$ is the normalized difference between discharge density and ambient density, l_M and l_Q are the characteristic length scales of momentum and volume flux, respectively, F_d and R_0 are the jet densimetric Froude number and Richardson number, respectively, Re is the jet Reynolds number, and the kinematic viscosity $\nu=10^{-6}$ m^2/s.

C. Vertical distribution of circulation and dynamics of buoyant jets

In the following two sections, a strategy is developed to determine the value of the formation number, or the critical value of formation time above which a trailing stem is maintained behind the leading vortex ring. The strategy to determine the formation number includes three steps: (a) identifying the starting vortex ring, (b) locating the pinch-off if and when it occurs, and (c) analyzing the circulations of both the whole computational domain and the vortex ring to quantify the development process.

First, we define a cross-sectional circulation to distinguish the vortex ring from the trailing jet-vortex ring system as follows:

$$\omega^*(z)=\int_{\mathrm{HCP}}\omega_y(x,z)dx,\tag{10}$$

where HCP represents the half central plane, i.e., either left central plane $(0<x<3D, y=3D)$, or right central plane $(3D<x<6D, y=3D)$, and ω_y represents the vorticity in the y direction. Figure 2 shows the vorticity field of the vortex ring formation process coupled with the vertical distribution of ω^* versus the penetration depth, z, for the case of Re=2500, $t_f=L/D=12$, and $R_0=0.186$. The peak of the absolute value of the cross circulation, $|\omega^*|$, indicates the position of the center of the starting vortex ring. Note that $|\omega^*|$ also has a relative maximum at the edge of the orifice generated by the free-slip boundary condition. At $tU_0/D=3$ and 5, the head vortex is well organized, followed by a trailing stem. At $tU_0/D=8$, the $|\omega^*|$ curve shows two minima behind the center of the head vortex, which indicates that another new vortex is forming at the leading edge of the trailing stem. At $tU_0/D=9$, this "leading-trailing vortex" gathers toward the central axis and

Downloaded 23 Feb 2010 to 171.67.216.23. Redistribution subject to AIP license or copyright; see http://pof.aip.org/pof/copyright.jsp

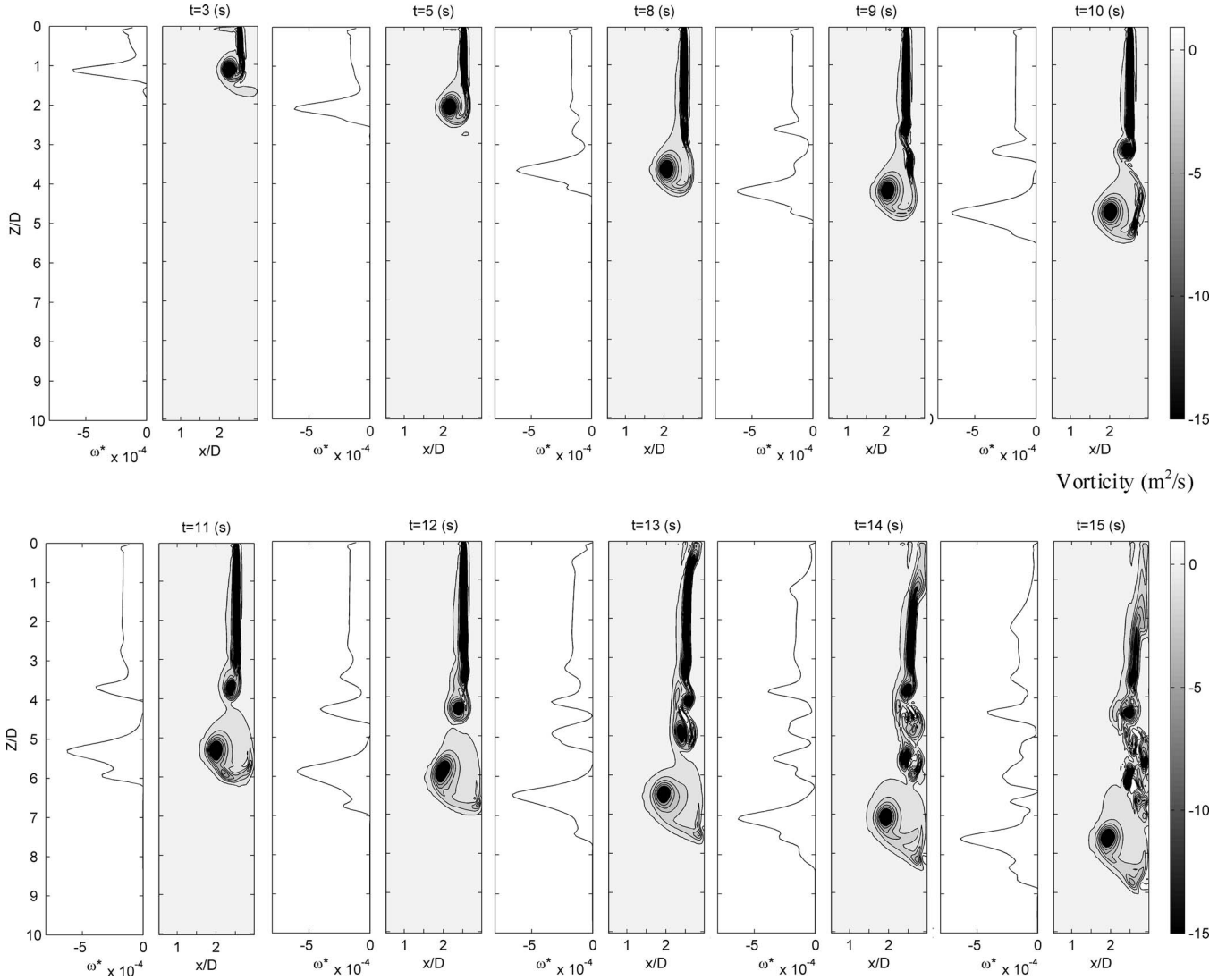

FIG. 2. The formation process of vortex ring/trailing jet and the corresponding cross-sectional circulation ω^*.

is being merged into the head vortex. Meanwhile, a new leading-trailing vortex is being produced behind. At $tU_0/D=10$, the absorbed vortices have merged completely with the head vortex ring. With the added circulation, the head vortex ring pushes forward and detaches from the trailing stem at $tU_0/D=11$ to complete the pinch-off process. Here, we consider the time between $tU_0/D=9$ and 10 to be the time of pinch-off when the circulation of the absorbed vortices is added into the head vortex ring. After the discharge ceases at $tU_0/D=12$, the orifice stops providing any additional momentum, and the trailing stem disintegrates into turbulent patches of remnant mass.

From Fig. 2, a minimum of $|\omega^*|$ can be found between the starting vortex and the trailing stem throughout the development process until the full turbulent flow is established. Specifically, this minimum always closely follows the center peak of the vortex ring. This minimum is used as the criterion to divide the flow field into: (1) the starting vortex region (below) and (2) the trailing stem region (above). Hereafter, the term "head vortex" refers to the starting vortex ring in order to differentiate it from "leading vortex," which is the regenerated vortex ring formed after the pinch-off (see Ref. 28). Note that a similar criterion has been used in Ref. 5 to show the onset of the jet instability and a radial vorticity distribution of the head vortex ring has been used in Ref. 6 to analyze the pinch-off dynamics.

D. Determination of buoyant formation number

Figure 3 shows the total and starting vortex circulations for the above case of Re=2500, $R_0=0.186$, and $t_f=12$, as a function of nondimensional time tU_0/D. [Note that because U_0 and D have the same magnitude (5 cm/s and 5 cm, respectively), tU_0/D and t are numerically equal.] Basically, the circulation progress can be categorized into two segments. When $0<tU_0/D<t_f$, the total circulation in the computation domain continuously increases due to the jet discharge; when $tU_0/D>t_f$, the addition by the discharge ceases, but the circulation in the domain continues to increase (though at a different rate) due to the buoyancy of the plume fluid already introduced. Therefore, the slope of the total circulation changes at $t=t_f$. The lower circulation curve

Downloaded 23 Feb 2010 to 171.67.216.23. Redistribution subject to AIP license or copyright; see http://pof.aip.org/pof/copyright.jsp

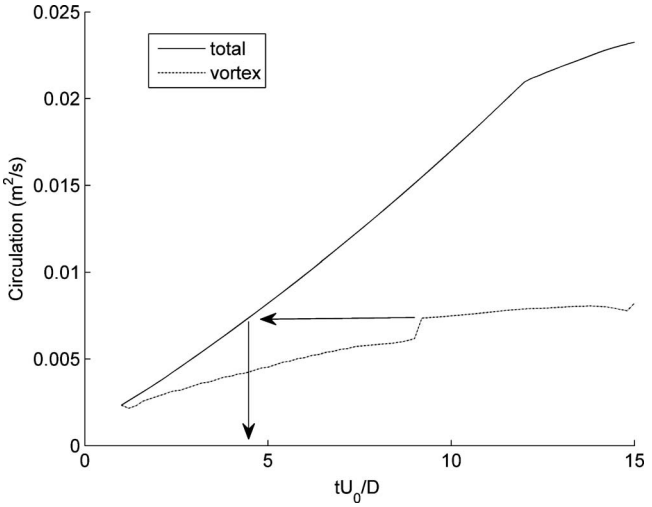

FIG. 3. The total and starting vortex circulation.

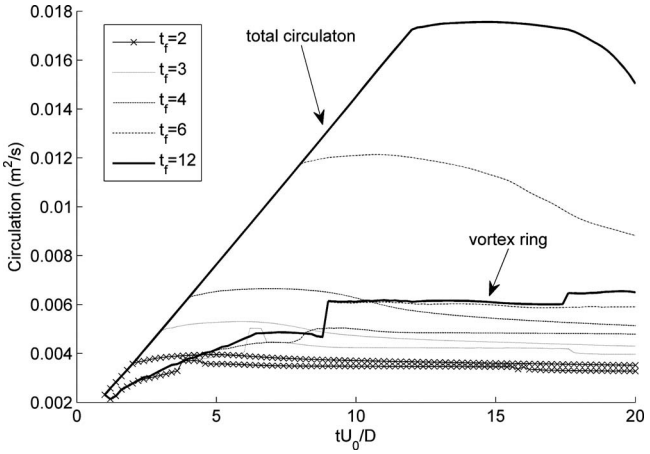

FIG. 4. The total and starting vortex circulation for pure jets with different formation times.

in Fig. 3 illustrates the entire development of the starting head vortex ring. The circulation of the starting vortex keeps increasing during the formation process fed by the trailing leading vortices. As discussed previously, the circulation of the starting vortex then experiences a step jump when the pinch-off occurs. After pinch-off, the vortex ring is separated from the trailing stem. Subsequently, it would lose the supply from the trailing stem and thus the circulation increase would slow to a magnitude corresponding to the buoyant action of the vortex itself.

Gharib *et al.*[2] proposed a method to determine the formation number of a starting jet by defining it based on the circulation of the starting vortex attaining a maximum. This method has been used by many subsequent studies (e.g., Refs. 4 and 5). For buoyant jets, however, this method cannot be used directly since the total circulation, as well as the circulation of the head vortex ring, continues to increase after pinch off due to the buoyancy of the plume fluids. Thus, we seek an alternative approach through the identification of the step jump in circulation that enables the head vortex to pinch off from the trailing stem.

The present strategy to determine the formation number is illustrated by the two arrows in Fig. 3. First, the circulation value after the step jump in circulation is distinguished. The intersection point on the total circulation line which has the same value is then noted. The corresponding time, indicated by the vertical downward arrow, is finally obtained as the formation number.

III. FORMATION NUMBER FOR STARTING PURE JETS

We perform numerical simulations with the configuration of a piston-driven pure jet for verification purposes. The evolution of the total and starting vortex circulations with different formation times is presented in Fig. 4. In the beginning, both the total and head vortex circulations increase linearly with time. Then, the total circulation becomes a constant after the discharge ceases at $tU_0/D=t_f$ and decreases gradually due to viscous dissipation (which is different from Fig. 3 in which buoyancy is present), while the head vortex circulation reaches another constant value earlier before a step jump occurs. The formation number can be identified to be 3.9 using the strategy discussed previously, which is consistent with the range of 3.6–4.5 found by Gharib *et al.*[2] The value is also close to the previous numerical predictions of 3.3 in Ref. 4 and 3.8 in Ref. 5, although their studies were restricted to the laminar range with symmetric vortex rings which differ significantly from the present simulations.

Two different vortex-stem systems with $t_f=L/D=3$ and 5 are shown in Fig. 5 to illustrate the absence and presence of the trailing stem, respectively. At $tU_0/D=3$, the vorticity fields of both cases have the same pattern in which the head vortex leads the stem at the same speed. At $tU_0/D=5$, the trailing stem with $t_f=3$ huddles together to form a leading-trailing vortex, which is subsequently absorbed into the starting vortex. In comparison, the starting vortex of $t_f=5$ is still supported by the trailing stem and keeps developing at $tU_0/D=5$. At $tU_0/D=8$, the vortex ring of $t_f=3$ has finished engulfing the trailing vortex and begun to decelerate due to viscous dissipation, while the starting vortex of $t_f=5$ has initiated the pinch-off process. At last, all the circulation is contained in the head vortex for $t_f=3$, whereas an obvious remnant is left for $t_f=5$. To show the quantitative differences, the cross-sectional circulations of the stem region between these two formation time cases are compared in Fig. 6. The circulation of $t_f=5$ is clearly higher than that of $t_f=3$ around $z=3D$ in the remnant region. This again indicates that a significant circulation is left in the remnant mass of the former, and reinforces the conclusion that the formation number falls between 3 and 5, which is consistent with the result of 3.9 obtained above.

IV. BUOYANT FORMATION NUMBER FOR BUOYANT JETS

The main objective of the current study is to investigate the effect of buoyancy on the formation process of starting buoyant jets. In the following, the LES simulation results of starting buoyant jets are presented. To begin, we shall first define the categories of buoyant jets based on the initial con-

Downloaded 23 Feb 2010 to 171.67.216.23. Redistribution subject to AIP license or copyright; see http://pof.aip.org/pof/copyright.jsp

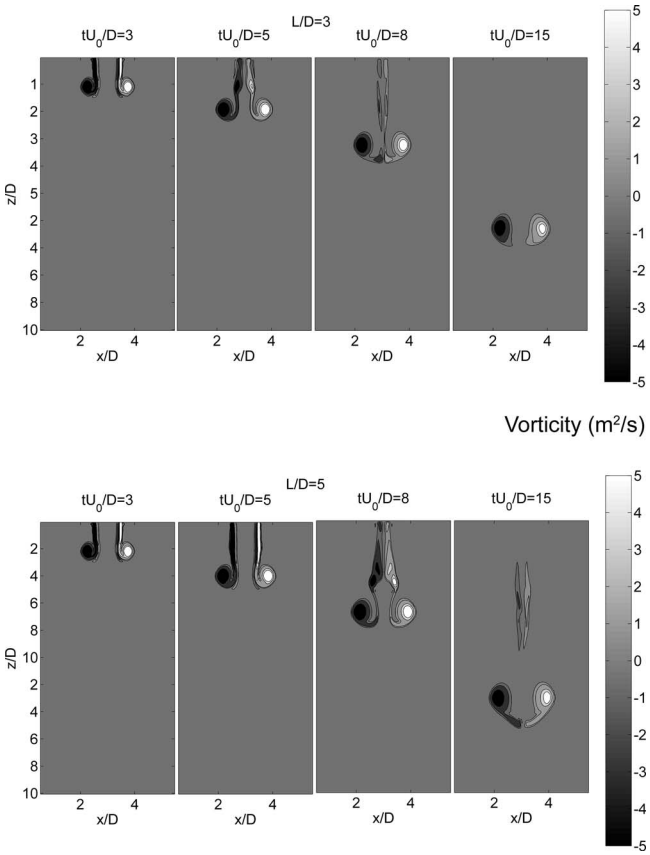

FIG. 5. Comparison of the vorticity fields for different formation times at the center plane.

ditions of the momentum and buoyancy fluxes at their source. Then, an example of the development of the buoyant jet is described to demonstrate the simulation results and the differences introduced by the buoyancy. Using the strategy detailed in Secs. II C and II D, the buoyant formation number, i.e., formation number incorporating the buoyancy effect, is determined covering the entire range of Richardson number from pure jet to lazy plume. Finally, a model is developed based on the slug model to predict the buoyancy influence on the formation process.

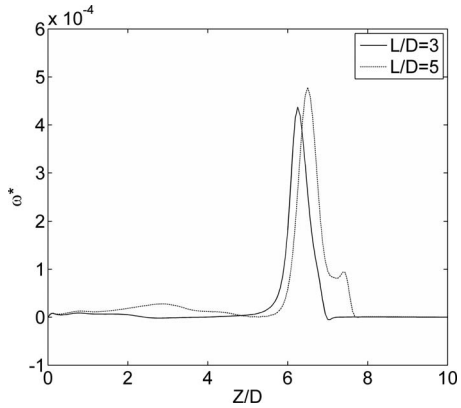

FIG. 6. Comparison of the cross-sectional circulations of starting pure jets at $t=15$ s.

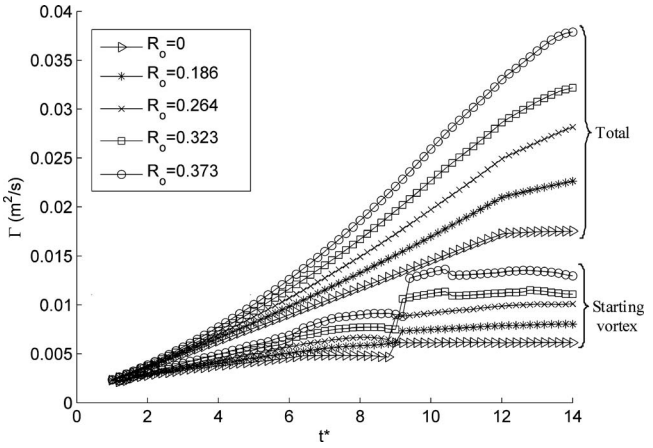

FIG. 7. The total and head vortex ring circulations under different buoyancy fluxes.

A. Richardson number and buoyant jets

Morton[29] suggested the following dimensionless source parameter to classify buoyant jets:

$$\Lambda = \frac{5Q_0^2 B_0}{4aM_0^{5/2}} = 12.3\frac{g'D}{U_0^2} = 12.3\frac{R_0^2}{(\pi/4)^{1/2}}, \tag{11}$$

where $a(=0.09)$ represents the entrainment coefficient. Using this source parameter, a pure jet (no buoyancy) can be defined with $\Lambda=0$, a buoyant jet for $0<\Lambda<1$, a pure plume for $\Lambda=1$, and a lazy plume for $\Lambda>1$. Since this parameter relates directly to the Richardson number, R_0, the definitions can be represented alternatively as $R_0=0$ for pure jets, $0<R_0<0.27$ for buoyant jets, $R_0=0.27$ for pure plumes, and $R_0>0.27$ for lazy plumes.

B. Numerical results

In the numerical simulations, the buoyancy flux is added into the discharge in an incremental manner. The total and head vortex ring circulations are shown in Fig. 7 based on the numerical simulations. According to this figure, the circulation is generally increased by the buoyancy flux, which is reflected in the steeper slope of the circulation lines. Consequently, the curves with the buoyancy flux deviate from the linear relationship of the pure jet in Fig. 7. The pinch-off times are shown to be the same in this figure. This implies that the effects of buoyancy and momentum fluxes are uncoupled, which has been observed in the analysis of the buoyant jet penetration rate.[25]

The effect of buoyancy on the formation number is shown in Fig. 8, where it can be observed that the formation number generally increases with the Richardson number. Note that the Richardson number in the present simulations covers a wide range from pure jet $(R_0=0)$ to lazy plume $(R_0>0.27)$. When R_0 reaches a large number of more than 1.0, the formation number cannot be clearly determined because irregular fluctuations are present in the circulation curves, flooding the step jump and destroying the characteristic of a constant maximum.

Downloaded 23 Feb 2010 to 171.67.216.23. Redistribution subject to AIP license or copyright; see http://pof.aip.org/pof/copyright.jsp

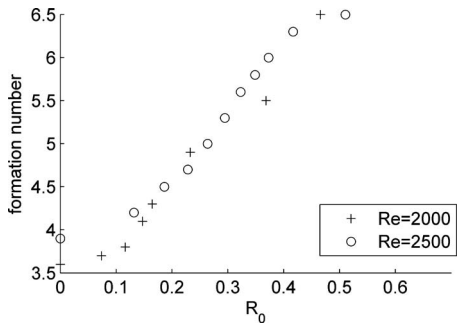

FIG. 8. The buoyant formation number as a function of Richardson number for two Reynolds numbers.

Based on the numerical results with the two source conditions of Re=2000 and 2500, the following best fit curve relating the formation number to the Richardson number can be obtained:

$$N_f = m\left[1 + \mathrm{erf}\left(\frac{R_0 - \mu}{\sqrt{2}\sigma}\right)\right] + N_{f_0}, \tag{12}$$

where the amplitude $m=1.3$, the standard deviation $\sigma=0.1$, the median $\mu=0.3$, and the formation number of the pure jet $N_{f_0}=4$.

Drawing on the similarity between pure jets and thermals, Shusser and Gharib[16] argued that a characteristic time scale, T_0, should be the time required for the jet or thermal to penetrate a distance of one nozzle diameter based on the velocity acquired at the instant when the jet or thermal has traveled one diameter (i.e., $T_0^{\mathrm{jet}}=D/U_0$ for a pure jet and $T_0^{\mathrm{ther}}=\sqrt{D/2g'}$ for a thermal, the latter calculated by assuming that the flow has acquired a kinetic energy per unit mass of $g'D$ at a vertical displacement D). Analyzing the experimental data of Lundgren *et al.*[30] for a laminar plume without initial momentum, they obtained the formation number as 4.73, somewhat larger than the traditional number of about 4. They attributed the larger value to the combined action of buoyancy inducement and momentum acceleration. Following the reasoning of Shusser and Gharib,[16] the time scale for a thermal can be established as $T_0=D/\sqrt{U_0^2+2g'D}$. This is the time characteristic time required for the buoyant jet to penetrate one diameter and is obtained by equating the kinetic energy of the flow at a distance D to the sum of the kinetic energies associated with the pure jet and the thermal. Consequently, a buoyant formation time can be defined as follows:

$$\tau_{\mathrm{jet}} = \frac{t}{T_0^{\mathrm{jet}}} = \frac{tU_0}{D}, \tag{13a}$$

$$\tau_{\mathrm{ther}} = \frac{t}{T_0^{\mathrm{ther}}} = \frac{t\sqrt{2g'}}{\sqrt{D}}, \tag{13b}$$

$$\tau = \frac{t}{T_0} = \frac{t\sqrt{U_0^2 + 2g'D}}{D}, \tag{13c}$$

The results for Re=2500 are transformed to the format of the buoyant formation number and shown in Fig. 9. It can be observed that the buoyant formation number is not a constant after the scaling of Eq. (13) and generally increases with larger buoyancy. Note that the present condition pertains to turbulent discharge at the source, which is contrary to thermals which are generally laminar near the origin; the difference between the present study and that of Shusser and Gharib[16] can thus be attributed in part to the distinctly different source conditions.

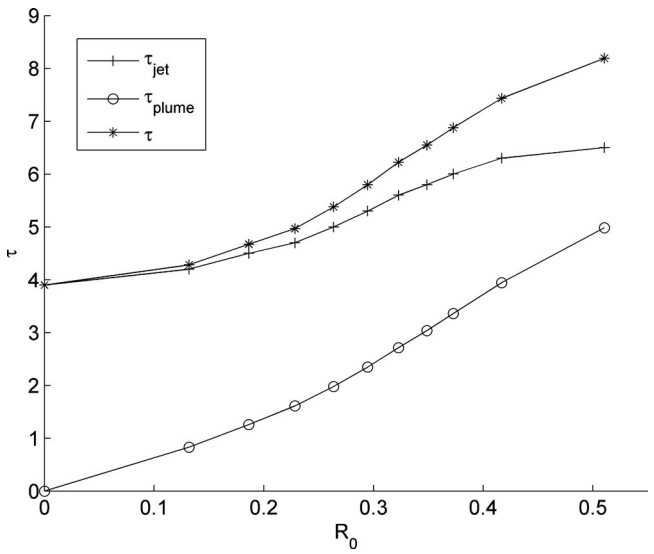

FIG. 9. The formation number as a function of the Richardson number.

C. Analytical model

As an analytical tool, the slug model proposed by Gharib *et al.*[2] and Mohseni and Gharib[8] for pure jets can be further developed for buoyant jets. The kinetic energy, circulation, and impulse of a pure jet can be approximated by the slug model as

$$E_1 = \tfrac{1}{8}\pi\rho D^2 L U_0^2, \tag{14}$$

$$\Gamma_1 = \tfrac{1}{2}U_0 L, \tag{15}$$

$$I_1 = \tfrac{1}{4}\pi\rho D^2 U_0 L, \tag{16}$$

where E_1 is the kinetic energy, Γ_1 is the circulation, I_1 is the impulse, and $L=U_0 t_f$ is the equivalent stroke of the piston. The addition of buoyancy flux changes the flow behavior in three aspects: (1) an excess kinetic energy of the buoyant jet can be generated from the transformation of the potential energy; (2) an excess circulation can be induced by the difference between the additional velocity due to buoyancy and the ambient fluid; and (3) the excess impulse is increased by the gravity force. We assume that the discharge fluid rolls up to form a vortex ring and half of its surface, $\frac{1}{2}\pi DL$, is exposed to the ambient quiescent fluid, where the circulation inducement occurs. The expression for kinetic energy, circulation, and impulse can thus be changed into

$$E = E_1 + E_2 = \tfrac{1}{8}\pi\rho D^2 L U_0^2 + \tfrac{1}{4}\pi\rho D^2 L g'\left(U_0 t + \tfrac{1}{2}g' t^2\right), \tag{17}$$

Downloaded 23 Feb 2010 to 171.67.216.23. Redistribution subject to AIP license or copyright; see http://pof.aip.org/pof/copyright.jsp

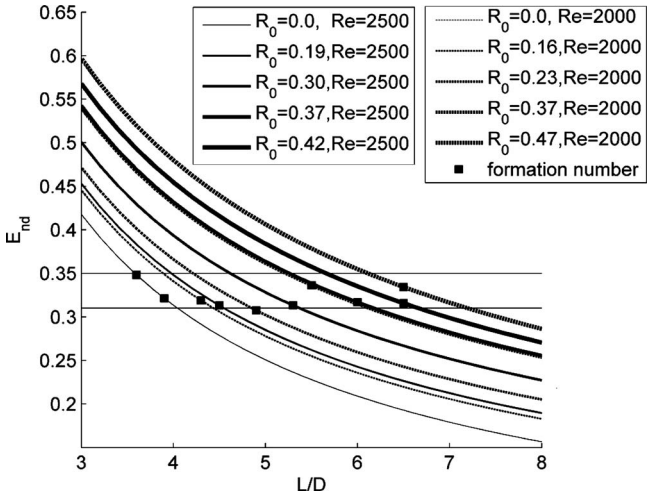

FIG. 10. Dimensionless energy for different buoyancy fluxes versus the formation time L/D.

$$\Gamma = \Gamma_1 + \Gamma_2 = \tfrac{1}{2}U_0 L + \tfrac{1}{4}Lg't, \tag{18}$$

$$I = I_1 + I_2 = \tfrac{1}{4}\pi\rho D^2 U_0 L + \tfrac{1}{4}\pi\rho D^2 Lg't, \tag{19}$$

where the subscript "2" refers to the gravitational effects.

Likewise, the dimensionless energy can be expressed as

$$E_{\mathrm{nd}} = \frac{E}{\rho^{1/2}\Gamma^{3/2}I^{1/2}} = \sqrt{\frac{\pi}{2}}\frac{D}{L}(1+\delta)^{3/2}, \tag{20}$$

where

$$\delta = \frac{g't}{g't + 2U_0}. \tag{21}$$

The coefficient δ is a function of time, which indicates that the buoyancy effect continuously increases the nondimensional energy E_{nd}. If we replace t by L/U_0,

$$\delta = \frac{g'L}{g'L + 2U_0^2} \tag{22}$$

and E_{nd} becomes the nondimensional energy at the end of a discharge. In this manner, E_{nd} would give the limiting value when L/D equals the formation number.

Based on the Kelvin–Benjamin variational principle, Gharib *et al.*[2] first proposed that the formation number for pure jets corresponds to $E_{\mathrm{nd}}=0.33$. This is confirmed by both numerical simulations and theoretical analysis.[4,5,8] Incorporating the buoyancy effect, we find that this limiting value is also applicable to the formation processes of buoyant jets. The dimensionless energy with different buoyancy and momentum fluxes is plotted against the formation time, L/D, in Fig. 10. The formation numbers determined by the numerical simulations are marked with solid squares in the same figure, which fall in a narrow region between $E_{\mathrm{nd}}=0.31$ and 0.35, with a median of 0.33. The results imply that the formation number can be predicted by the intercepts of $E_{\mathrm{nd}}=0.33$ and the curves for different buoyancy fluxes. In other words, $E_{\mathrm{nd}}=0.33$ is still valid for starting buoyant jets.

In the asymptotic case of a pure jet with $g'=0$ and $\delta=0$, E_{nd} is consistent with the model used previously in the literature for pure jets, which corresponds to $L/D \approx 4$ as expected. With $g'=\infty$, however, $\delta=1$, and the formation number has an upper limit of $L/D=10.7$. This implies the interesting result that the ability of buoyancy to enhance circulation and delay pinch-off is restricted by a maximum stroke length of $10.7D$.

V. SUMMARY AND CONCLUSIONS

The present study examines the formation process of the buoyant jet over a wide range from a pure jet to a thermal. To determine the formation number, a method to differentiate the head vortex ring and the trailing stem is derived based on the evolution of the cross-sectional circulation. Because the buoyancy flux continuously induces the circulation, a new strategy is proposed to identify the formation number using the observed step jump in the vortex ring circulation. The strategy is validated by the results that it is able to reproduce the formation number of a pure jet. In addition, the relationship between the presence of the trailing stem and the formation number is also reconfirmed.

Numerical simulations are performed by adding buoyancy flux incrementally to simulations with two turbulent source conditions of Re=2000 and 2500. Results show that the buoyant formation number increases with the Richardson number following an error function relationship [Eq. (12)]. In addition, since the momentum and buoyancy effects are uncoupled at the initial development of the buoyant jet, the time for the step jump occurrence is found to be invariant through the range of added buoyancy flux. To bridge the gap between the time scaling of pure jets and plumes, a buoyant time scale is formulated. Finally, with a slug model that incorporates the buoyancy effect as well as the Kelvin–Benjamin variational principle, the buoyant formation number is shown to follow the nondimensional energy of 0.33, which is consistent with the value for pure jets that was reported in the literature.

While this paper was in press, Marugán-Cruz *et al.*[31] reported that for negatively buoyant starting jets, the formation number decreases with increasing negative buoyancy. This conclusion is consistent and mirrors our findings here that the formation number increases with increasing positive buoyancy. It also implies a potential extension of our analysis, which we are pursuing, to encompass the entire range of density deficit of the injection fluid from positive to negative.

ACKNOWLEDGMENTS

This work was supported by the Singapore National Research Foundation (NRF) through the Singapore-MIT Alliance for Research and Technology (SMART) Center for Environmental Sensing and Modeling (CENSAM). The first author wishes to acknowledge Mr. Yi-ju Chou for help in parallel computing.

[1] Y. Fukumoto, "Global time evolution of viscous vortex rings," Theor. Comput. Fluid Dyn. (2009), http://www.springerlink.com/content/u30t3p6072832634.
[2] M. Gharib, E. Rambod, and K. Shariff, "A universal time scale for vortex ring formation," J. Fluid Mech. **360**, 121 (1998).

Downloaded 23 Feb 2010 to 171.67.216.23. Redistribution subject to AIP license or copyright; see http://pof.aip.org/pof/copyright.jsp

[3]K. Shariff and A. Leonard, "Vortex rings," Annu. Rev. Fluid Mech. **24**, 235 (1992).
[4]M. Rosenfeld, E. Rambod, and M. Gharib, "Circulation and formation number of laminar vortex rings," J. Fluid Mech. **376**, 297 (1998).
[5]W. Zhao, S. H. Frankel, and L. G. Mongeau, "Effects of trailing jet instability on vortex ring formation," Phys. Fluids **12**, 589 (2000).
[6]K. Mohseni, H. Ran, and T. Colonius, "Numerical experiments on vortex ring formation," J. Fluid Mech. **430**, 267 (2001).
[7]J. O. Dabiri and M. Gharib, "Fluid entrainment by isolated vortex rings," J. Fluid Mech. **511**, 311 (2004).
[8]J. J. Allen and T. Naitoh, "Experimental study of the production of vortex rings using a variable diameter orifice," Phys. Fluids **17**, 061701 (2005).
[9]K. Mohseni and M. Gharib, "A model for universal time scale of vortex ring formation," Phys. Fluids **10**, 2436 (1998).
[10]P. F. Linden and J. S. Turner, "The formation of vortex rings, and the efficiency of propulsion devices," J. Fluid Mech. **427**, 61 (2001).
[11]K. Mohseni, "Statistical equilibrium theory for axisymmetric flows: Kelvin's variational principle and an explanation for the vortex ring pinch-off process," Phys. Fluids **13**, 1924 (2001).
[12]F. B. Kaplanski and Y. A. Rudi, "A model for the formation of 'optimal' vortex rings taking into account viscosity," Phys. Fluids **17**, 087101 (2005).
[13]M. Shusser, M. Rosenfeld, J. O. Dabiri, and M. Gharib, "Effect of time-dependent piston velocity program on vortex ring formation in a piston/cylinder arrangement," Phys. Fluids **18**, 033601 (2006).
[14]T. Benjamin, "The alliance of practical and analytical insights into the nonlinear problems of fluid mechanics," *Applications of Methods of Functional Analysis to Problems in Mechanics* (Springer, Berlin, 1976), pp. 8–29.
[15]T. S. Pottebaum and M. Gharib, "The pinch-off process in a starting buoyant plume," Exp. Fluids **37**, 87 (2004).
[16]M. Shusser and M. Gharib, "A model for vortex ring formation in a starting buoyant plume," J. Fluid Mech. **416**, 173 (2000).
[17]H. Wang and A. W. K. Law, "Second-order integral model for a round turbulent buoyant jet," J. Fluid Mech. **459**, 397 (2002).
[18]Y. Zang, R. L. Street, and J. R. Koseff, "A non-staggered grid, fractional step method for time-dependent incompressible Navier-Stokes equations in curvilinear coordinates," J. Comput. Phys. **114**, 18 (1994).
[19]Y. Zang, "On the development of tools for the simulation of geophysical flows," Ph.D. thesis, Stanford University, 1995.
[20]M. V. Salvetti, Y. Zang, R. L. Street, and S. Banerjee, "Large-eddy simulation of free-surface decaying turbulence with dynamic subgrid-scale models," Phys. Fluids **9**, 2405 (1997).
[21]B. P. Leonard, "A stable and accurate convective modelling procedure based on quadratic upstream interpolation," Comput. Methods Appl. Mech. Eng. **19**, 59 (1979).
[22]A. Cui and R. L. Street, "Large-eddy simulation of coastal upwelling flow," Environ. Fluid Mech. **4**, 197 (2004).
[23]Y. Zang and R. L. Street, "Numerical simulation of coastal upwelling and interfacial instability of a rotating and stratified fluid," J. Fluid Mech. **305**, 47 (1995).
[24]L. L. Yuan, R. L. Street, and J. H. Ferziger, "Large-eddy simulations of a round jet in crossflow," J. Fluid Mech. **379**, 71 (1999).
[25]R. Q. Wang, A. W. K. Law, E. E. Adams, and O. B. Fringer, "Large eddy simulation of starting buoyant jets," Phys. Fluids (submitted).
[26]L. L. Yuan, "Large eddy simulations of a jet in crossflow," Ph.D. thesis, Stanford University, 1997.
[27]H. B. Fischer, *Mixing in Inland and Coastal Waters* (Academic, New York, 1979).
[28]A. W. K. Law, J. Ai, and S. C. M. Yu, "Leading vortex of a starting forced buoyant plume," *Proceedings of the Ninth Asian Symposium on Visualization*, edited by C. T. Hu and H. H. Qiu, Hong Kong, China, 4–6 June 2007 (IOS, Amsterdam, 2007).
[29]B. R. Morton, "Forced plumes," J. Fluid Mech. **5**, 151 (1959).
[30]T. S. Lundgren, J. Yao, and N. N. Mansour, "Microburst modelling and scaling," J. Fluid Mech. **239**, 461 (1992).
[31]C. Marugán-Cruz, J. Rodríguez-Rodríguez, and C. Martínez-Bazán, "Negatively buoyant starting jets," Phys. Fluids **21**, 117101 (2009).

Downloaded 23 Feb 2010 to 171.67.216.23. Redistribution subject to AIP license or copyright; see http://pof.aip.org/pof/copyright.jsp